MULTI-HYPOTHESIS LIGHT CURVE INVERSION SCHEME FOR CONVEX OBJECTS WITH MINIMAL OBSERVATIONS

S. Fan and C. Frueh

School of Aeronatuics and Astronautics, Purdue University, West Lafayette IN 47906, USA,
Email: {fan11, cfrueh}@purdue.edu

ABSTRACT

Knowing the exterior shape forms an important piece of information for space debris in the near-Earth region. It has been demonstrated in the past that the photometric measurements, also known as the light curve, contains the shape information. Previous work by the authors has established a shape estimation framework that is capable of generating high accuracy candidates for simple objects. For this work, an alternative multi-hypothesis framework is proposed based on a kind of particle filter using sequential importance resampling. Under realistic measurement noise setting, the simulation result has shown that likely candidates can be obtained up to satisfactory recognition with quantitative measure provided.

Keywords: Light Curve; Shape Estimation; Inversion Problem; Extended Gaussian Image; Multi-Hypothesis; Particle Filter; Convex Objects; Minkowski Problem.

1. INTRODUCTION

Traditionally, the orbit information (dynamic states) for objects in space has been of interest and it is obtained by solving the orbit determination problem. In recent years, it has been realized that knowing the exterior shape also forms an important piece of information, especially for space debris. The shape is coupled with the object's orbit via non-conservative forces, which is integral to orbital predictions as they pose a significant influence on Earth-orbiting human-made objects. Additionally, future missions involving close-up investigation of these objects have also promoted the necessity of characterizing their shapes.

Although RADAR system has been used to monitor space debris with good potential in resolution during direct imaging [7, 15]. Due to the relatively flexible deployment and robust operation, an effective way to observe the space debris population is the use of ground-based optical sensors.

Optical observation for objects in GEO has been conducted by Schildknecht et al. [17, 18], which brings awareness to the explosion events that happened in geostationary transfer orbits (GTO). Silha et al. [19] conducted a similar space debris survey in medium Earth orbits (MEO) and concluded that one uncorrelated object could be identified for every 100 minutes of observations. The National Aeronautics and Space Administration (NASA) and the Air Force Maui Optical and Supercomputing Site (AMOS) together conduct the debris measurement program focusing on the LEO and GEO region in both visible and infrared spectrum.

An information gathered during optical observation beyond the angular position, is the object's brightness. The so-called light curve refers to the change of brightness as a function of time. When the object is not illuminating by itself, the brightness is dependent on solar activity, orbits, attitude motion, exterior shape, material, atmosphere, and other attenuating factors. In the past, it has been shown that the shape information can be extracted from photometric measurements under assumptions [8, 10, 11, 12, 9].

At the scale of space debris, however, the measurement can be heavily influenced by noise given their sheer size, altitude, and reflection property. An approach that is capable of estimating shapes in this scenario is required. The authors had previously proposed using Monte Carlo simulation and a direct multi-hypothesis scheme to explore the solution space when assuming an object's orbit and attitude motion [4]. The main advantage of a multi-hypothesis framework is that it provides a conclusive statement on shape candidate's likelihood. In this article, particle filtering is implemented to sequentially update candidates while incorporating follow-up observations.

2. THEORY

This section first introduces the typical light curve inversion problem described by Kaasalainen et al. [10, 11], which takes observation data as input and produce a shape candidate as output after going through the two-step inversion process. The Monte Carlo noise sampling

Proc. 8th European Conference on Space Debris (virtual), Darmstadt, Germany, 20–23 April 2021, published by the ESA Space Debris Office
Ed. T. Flohrer, S. Lemmens & F. Schmitz, (http://conference.sdo.esoc.esa.int, May 2021)

$$\Lambda_{n-plate}(t_j) = \sum_{\lambda}\sum_{i=1}^{n} \frac{A_i}{\pi r^2_{topo,i,j}} (\hat{N}_{i,j}\cdot\hat{S}_{i,j})\mu'_{0,i,j}\left[C_{d,i}(\lambda)(\hat{N}_{i,j}\cdot\hat{O}_{i,j}) + \pi\tau_{i,j}\beta_{i,j}\frac{C_{s,i}(\lambda)d^2_{Sun}}{a^2_{Sun,i,j}}\right] \tag{2}$$

$$\mu'_{0,i,j} = \begin{cases} 1, \text{ if } (\hat{N}_{i,j}\cdot\hat{O}_{i,j}) \geq 0 \\ \quad \text{and } (\hat{N}_{i,j}\cdot\hat{S}_{i,j}) \geq 0 \\ 0, \text{ else} \end{cases} \tag{3}$$

$$\tau_{0,i,j} = \begin{cases} 1, \text{ if } 1-\cos(0.25^{o}) \leq \frac{\hat{O}+\hat{S}}{|\hat{O}+\hat{S}|}\cdot\hat{N} \leq 1+\cos(0.25^{o}) \\ 0, \text{ else} \end{cases} \tag{4}$$

process which establishes the initial set of candidates, is then briefly explained. For a more detailed description of the method, the reader can refer to the previous publication by the authors [4]. Finally, the particle filter application is proposed along with detailed treatment on the Extended Gaussian Image (EGI). Part of the treatment leverages a quantitative measure that bounds the deviation among convex objects by Oliker and Frueh [16].

2.1. Light Curve Simulation

All light curves used in this article are simulated measurement. The simulation framework is proposed by the authors. The derivation and operation detail is described in [3]. A brief overview is provided here.

$$mag = m_{\text{Sun}} - 2.5 log_{10}\Lambda \tag{1}$$

The unit of relative magnitude is used in this study and the absolute magnitude of the Sun m_{Sun} is taken to be -26.74. Λ is referred to as the phase function which refers to the ratio of brightness (in irradiation) between the object and the Sun. The phase function function can be computed in an finite-element fashion for convex objects as Equation 2.

Equation 2 sums through the surface of convex object and wavelength λ, at each time index j. The convex object is consisted of n number of facets, each with area A_i and unit normal vector $\hat{N}_i$. The Lambertian and specular reflection coefficient is denoted by C_d and C_s. The vector $\hat{S}$ and $\hat{O}$ points towards the Sun and the observer respectively. Coefficient β refers to the ratio of the Sun disk to the reflective surface. The distance between facet and the Sun is d_{Sun}, and Solar radius is a_{Sun}. The topological distance is given by r_{topo}. Lastly, the parameter μ'_0 and τ_0 refers to the illumination and specular reflection condition for each facet per time.

2.2. Two-Step Inversion Process

The basic light curve inversion problem starts with a least square minimization problem as Equation 5.

$$Min \quad J = |L - \mathbf{G}a|^2 \tag{5}$$

$$Subject\ to \quad a_i \geq 0, \quad i = 1, ..., m \tag{6}$$

Column vector L refers to the series of photometric measurements of the size l-by-1. It is also the input of the equation. The output of the problem is the column vector a of the size m-by-1. Each element of a represents the albedo-area value associated with a certain normal-facing direction, where the list of normal directions is pre-sampled thus known. When assuming full knowledge on orbits and attitude motion, $\mathbf{G}$ matrix (size l-by-m) can be computed with known normal facing directions. A minor assumption here is that the distance between the object center of mass and support location, is ignored as they form part of the shape information.

An important remark here lies on the observability, or the rank condition on the matrix $\mathbf{G}$. A full rank matrix guarantees a unique answer to the least square problem. For the shape estimation problem, however, the rank condition is dependent on the observation geometry, namely, the orbit and the attitude motion. If a side of the object is not observed, the albedo-area associated is subsequently not subject to data but other conditions (like constraints for example). Friedman et al. [5] has shown that it is possible to arrange an observation plan for the purpose of shape estimation such that it guarantees full observability. For preliminary studies using computer simulations, implementing torque-free motion often suffice.

After obtaining the albedo-area vector a and associating it with the list of pre-sampled normal vectors, it forms the so-called Extended Gaussian Image (EGI). The EGI is referred to as a shape descriptor, which describes a closed three-dimensional surface in an alternative space. In our case where a numerical process is performed and data is discrete, a discrete EGI is used to represent a polyhedron or a 3-dimensional polytope.

Under the assumption of uniformity, a convex object is represented uniquely by an EGI. Assuming an object to be convex, to obtain the shape in three-dimensional Euclidean space from the EGI input is referred to as the shape reconstruction process. The process can be summarized as first solving the EGI optimization problem to obtain the support, and perform half-space intersection to bound the dual object. The shape is finally retrieved after applying the dual transform. An important note here is its sensitivity. Theoretically, the EGI input has to satisfy the condition of closeness and convexity. If a small disturbance is present in the input, the reconstruction process will be forced to add a small piece of non-zero area fac-

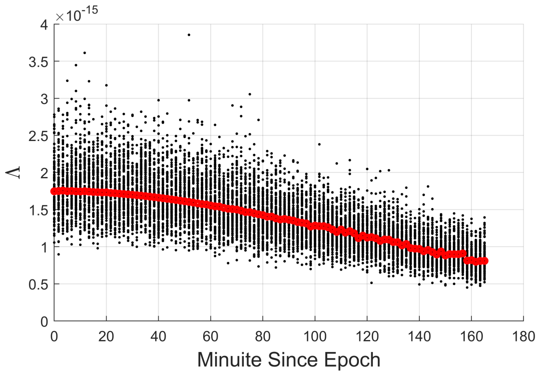

Figure 1. Demonstration of the noise sampling process, red dots: reference light curve simulated using setup from Section 3 on July-1-2018; black dots: 100 noisy light curves sampled at a signal-to-noise ratio of 5.

ing some direction and causes skewness to the result. A thresholding and smoothing stage can be added prior to this stage in order to reduce the problem's stiffness. They can are discussed in Section 2.4.

2.3. Monte Carlo Noise Sampling

When treating light curve data L as reference, noise can be sampled on top of the given data as the following.

$$\tilde{L} = L + \nu \tag{7}$$

For the scope of this article, noise ν is modeled as Gaussian noise with zero mean and constant standard deviation over all exposures. In reality, the noise will vary and is dependent on the signal itself. As noise is sampled and arbitrary number of noisy light curves are obtained, an equal number of EGIs are output by solving Equation 5. The noise sampling process is demonstrated in Figure 1

2.4. EGI Thresholding and Smoothing

For the least square problem (Equation 5) to be linearly independent, a full rank $\mathbf{G}$ matrix is ideal and the number of rows is greater than the number of columns, i.e. $l \leq m$. For non-trivial objects, one would expect there is a sufficient number of pre-sampled normal vectors such that the resolution of shape outcomes can be guaranteed. In practice, due to the discrete nature of the problem setup as well as different sources of noise, vector a will be obtained in a fashion that hardly has any zero entry. This poses a challenge for shape reconstruction as the process is highly sensitive to input.

Thresholding refers to the operation of discarding entries if they are below some fixed level. It is an effective way to suppress an overwhelming number of shape outcomes by focusing on the significant entries in vector a. It has to be emphasized that thresholding can be exercised at different levels of stringency during different operations. During the sequential importance resampling where the EGI is being constantly updated at each step according to new observations, the thresholding can be applied to include only the top 20 to 30 significant peaks for example. Whereas if there is a most likely EGI, a wider search would be more reasonable.

As mentioned in Section 2.2, the closeness and convexity condition is required for perfectly honest shape reconstruction. Since EGI lacks the information on support, it is difficult to perform a thorough check on the necessary conditions as far as the authors know. To reduce the stiffness when subject to input error, a smoothing stage is proposed as Equation 8 which aims to satisfy the necessary condition for closeness.

$$Min \qquad J = \| \sum_{i=1}^{m} \vec{n}_i (a_i + d_i) \| \tag{8}$$

$$Subject\ to \qquad 0 \leq d_i \leq u_i, \quad i = 1, ..., m \tag{9}$$

Equation 8 seeks the appropriate change in entries of vector a such that the expression is close to 0. The change in each entry is represented by d_i and it is bounded by upper limit u_i. The problem remains, as to if the post smoothing EGI is closer to the true EGI. However, the primary objective here is to let the reconstructed result honestly reflects the EGI input, at the cost of possibly losing some accuracy in terms of EGI.

2.5. C_2

Oliker and Frueh [16] proposed the following inequality to bound the deviation between two convex objects T_0 and T_1.

$$\sigma(\tilde{T}_0, \tilde{T}_1) \leq C\{\frac{V_1(T_0, T_1)}{V^{2/3}(T_0)V^{1/3}(T_1)} - 1\}^{1/3} \tag{10}$$

$$C = 2(\frac{R_0}{r_0})^2(\frac{R_0}{r_0} + \frac{R_1}{r_1}) \tag{11}$$

$$C_2 = C\{\frac{V_1(T_0, T_1)}{V^{2/3}(T_0)V^{1/3}(T_1)} - 1\}^{1/3} \tag{12}$$

The volume of T_0 is represented by $V(T_0)$ and $V_1(T_0, T_1)$ refers to the mixed volume of the two objects. R is the radius of smallest sphere that can enclose the object, and r is the radius of the largest sphere respectively. Here, the overall number on the right hand side is denoted by C_2. The quantity only bounds the difference and therefore should only be viewed as a general guideline.

2.6. Sequential Importance Resampling

From previous work [4], it has been established that shape estimation is possible for simpler objects with a relatively lower number of EGI directions, thus observations. For more complex objects, as to be seen in Section 3, the size of vector a is required to be at least on the level of thousands. When examining the problem from an estimation point of view, particle filtering [2] was recognized as an option.

Conventional estimation filters like Kalman filter and Markov model, has the advantage of mathematical tractability when applying assumptions [20]. When the noise is non-Gaussian and the analytical model is not possible with high dimensionality, different estimation schemes were proposed. A class of method is called Sequential Monte Carlo (SMC) method [14]. The center idea is to draw samples from a predicted distribution before new observations become available. It is sometimes called a simulated-based method which has flexible implementation.

When it is not convenient to draw such samples, a classical method called the importance sampling can be used [6] which aims to translate between the so-called importance distribution and the posterior distribution. Lastly, resampling stage is often mentioned to avoid degeneracy and improve efficiency [14, 13, 1].

In this work, the method of sequential importance resampling is thought to be viable for two main reasons. The first is the problem's dimension. For arguably complex objects, thousands of albedo-area entries are to be found as mentioned above. Limited by the computation resources today, to directly sample these entries will not be possible. The second is the sheer complexity when creating samples of vector a directly.

In fact, the Monte Carlo noise sampling process already solves part of the problem by operating on the light curve and then optimize for the albedo-area vector. The white noise in Equation 7 can be viewed as equal likely perturbed light curves, and the EGI obtained will be of equal importance as well. This has to do with the difficulty of inverting the $\mathbf{G}$ matrix in essence, where the observation matrix is basically of inclusion.

Particle filtering is also capable of incorporating new observations and updating particles. Both features are important for the light curve inversion problem. The operation with particle filtering application is summarized in Figure 2.

The process is initialized with the same Monte Carlo noise sampling process described in Section 2.3 as step 1, where N candidate shapes (particles) with equal importance are produced. Note that one shape is constructed from one EGI and a corresponding threshold, this number is therefore caused by both the number of EGI from light curve optimization as well as the thresholding process. In case of new observation, full knowledge of the orbit and attitude motion is also assumed. The light curve can be predicted for each particle at the time and location of y_2. Then the sequential process can start to incorporate further follow-up observation. The operation is outlined as the following:

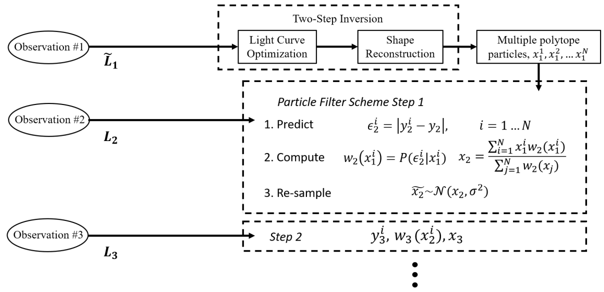

Figure 2. Sequential Importance Resampling Flow Chart

1. Particles from Monte Carlo noise sampling process, $x_1^1, \dots x_1^N$.
2. Predict light curve at follow-up location for previous particles, $y_2^1, \dots, y_2^N$.
3. Compare predicted light curve with the given follow-up light curve (y_2) and produce residue $\epsilon_2^1, \dots, \epsilon_2^N$.
4. Compute residue distribution and fit non-parametric probability distribution function, and compute importance (likelihood) of each particle based on their residue in the distribution.

$$w_2(x_1^i) = P(\epsilon_2^i | x_1^i) \tag{13}$$

$$w_2^0 = \sum_{i=1}^{N} w_2(x_1^i) \tag{14}$$

5. After applying normalizing factor w_2^0, a single EGI candidate (x_2) will be formed through a weighted mean of all previous particles and their updated importance.

$$x_2 = \frac{1}{w_2^0} \sum_{i=1}^{N} w_2(x_1^i) x_1^i \tag{15}$$

6. Re-sample x_2 in each of the EGI direction by adding Gaussian noise (with some standard deviation up to user specification), and create a new set of particles, $x_2^1, \dots x_2^M$.
7. Predict light curve at follow-up location for new particles, $y_3^1, \dots, y_3^M$.
8. Go to step 3 and repeat the process for next follow-up observations $y_3, y_4, \dots$, where M does not necessarily equal to N and varies at each iteration.

3. SIMULATION RESULTS

To demonstrate the effectiveness of the proposed method, a simulation scenario is established. An object is placed in orbit. Its light curve is simulated for the duration of the proposed observation period. The noise-affected light

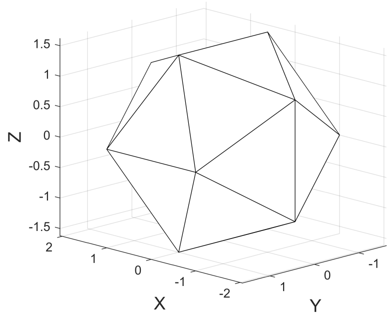

Figure 3. Icosahedron used for simulation, edge length: 2 m, surface area: 34.6 m^2

curve act as input to the inversion framework and the methodology is then carried out to examine the output.

A regular polyhedron of icosahedron is used which means the three-dimensional object consists of 20 identical faces. Each edge has a length of 2 m, and the total volume is 34.6 m^2. The object is assumed to have a uniform Lambertian reflection coefficient of 0.7 with specular component ignored.

A 60-degree inclined medium Earth orbit (MEO) at 20,000 km altitude is propagated. The first observation period is from June-1-2018 0 AM for 24 hours, 1350 evenly-spaced observations at a constant signal-to-noise (SNR) of 10 are assumed. The follow-up observation is set to take place a month later from July-1-2018 0 AM and lasts for 123 minutes. During this period, there are 5 sets of observations at a 10-minute separation from each other. Each set has 100 observations with a constant SNR of 5. A torque-free attitude motion is assumed which guarantees full observability. The ground observer is placed at the Purdue Optical Ground Station (POGS) located in New Mexico, USA.

Before demonstrating particle filtering, Figure 4 shows a collection of most likely EGIs. The reference EGI is plotted in red arrows. The 8 most likely EGIs are obtained by directly comparing with a noise sampled follow-up light curve (100 measurements at similar spacing) and the top 8 candidates with the least error are selected. Thus, all candidates are straight from the light curve optimization using the identical initial observation without any updating process.

It can be seen that only partial agreement is possible between candidate EGIs and the truth in terms of the density of arrows. Even with multiple follow-up noisy observations, the quality of individual candidate does not abet the characterization unless the information is combined in a meaningful way. Next, the update process with particle filtering is examined.

Figure 5 and Figure 6 shows candidates obtained after in-

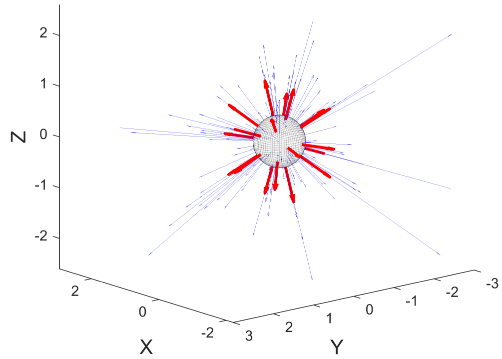

Figure 4. Simulation result after incorporating the first set of follow-up observation, 8 candidates (due to thresholding) are shown. C_2 value is computed with respect to the truth.

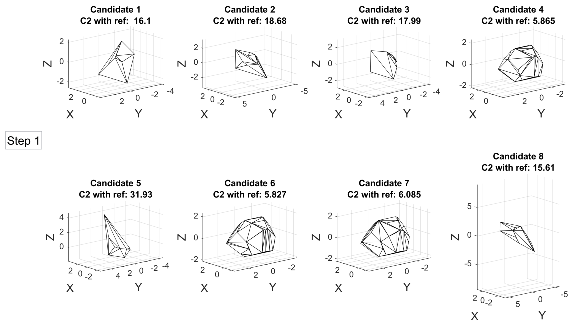

Figure 5. Simulation result after incorporating the first set of follow-up observation, 8 candidates (due to thresholding) are shown. C_2 value is computed with respect to the truth.

corporating the first and the fifth follow-up observation. Within the same figure, different shape candidates are constructed according to the same EGI at different thresholds, where the EGI leverages the proposed sequential importance resampling technique and therefore contains all the information up to the specific iteration.

Since C_2 is computed with respect to the truth, the quality of results is thus directly implied. Figure 6 shows that the list of candidates obtained in the last step is more likely to be closer to the truth. Several candidates also appear to be in the better aspect via visual inspection. In a real application, the knowledge about the truth can not be assumed. An alternative method is proposed here. That is for a specific likely EGI, to compute the C_2 value for each candidate with respect to all other candidates and form a matrix of C_2 values.

Table 1 prints an example C_2 table for all candidates shown in Figure 6. Note that candidate 3, 6, 7, and 8 coincide with the four shapes that have the lowest C_2 with respect to the reference. Here, a hypothesis which remains

Table 1. Example cross C_1 matrix printed according to the 8 candidates in Figure 6, rounding to decimal, colored column indicate likely candidates.

C_2	T_1	T_2	T_3	T_4	T_5	T_6	T_7	T_8
T_1	0.0	80.5	201.5	303.6	421.5	209.0	213.0	217.5
T_2	38.7	0.0	193.5	293.3	408.5	200.8	204.7	209.1
T_3	34.1	34.5	0.0	29.8	45.5	12.7	13.8	14.8
T_4	218.5	220.1	123.8	0.0	159.2	128.8	132.0	135.6
T_5	662.1	666.2	393.7	342.7	0.0	408.6	416.8	426.0
T_6	29.8	30.2	3.8	25.2	39.9	0.0	6.8	8.8
T_7	31.4	31.8	4.8	26.5	42.1	3.3	0.0	7.5
T_8	33.7	34.2	5.7	28.4	45.5	4.5	3.6	0.0

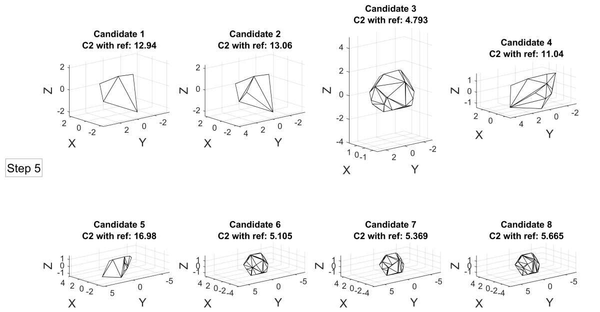

Figure 6. Simulation result after incorporating the fifth set of follow-up observation, 8 candidates (due to thresholding) are shown. C_2 value is computed with respect to the truth.

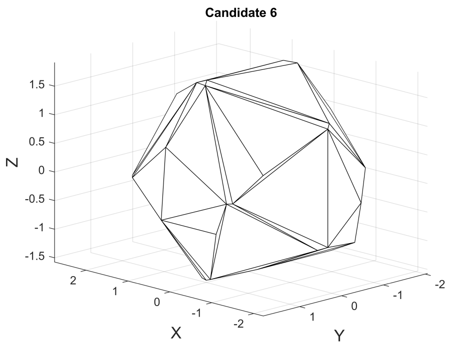

Figure 7. Best shape candidate after incorporating the fifth set of follow-up observation, selection according to C_2 matrix.

to be verified is that, a specific candidate that resembles closely to all other candidates is also the shape closest to the truth. For a more thorough investigation of a most likely candidate, the search is expanded to a wider range of thresholds. The final candidate is shown in Figure 7.

Since the order of convex objects does not commute for C_2 computation, the lower value should be used when comparing C_2 values between two objects. Among the four likely candidates, candidate 6 appears to be closer to all other candidates and is therefore selected as the winner.

4. CONCLUSION

A new light curve inversion method is proposed by applying particle filtering technique to the problem. Similar to the previous method proposed by the authors, the framework assumes no additional information on the object's shape beyond its orbit and attitude motion, and is capable of offering a quantitative conclusion on the candidate's likelihood. The new method, however, has the advantage of being sequential and updating candidates as new observations are being taken in. Based on the simulation results, the method is capable of outputting shape candidates up to satisfactory recognition, subject to noisy observations. Additionally, a selection criterion based on C_2 is proposed to further differentiate among candidates due to different thresholds.

ACKNOWLEDGMENTS

The work was supported via AFOSR BAA Grant FA9550-18-1-0154DEF.

REFERENCES

1. Doucet, A. On sequential simulation-based methods for bayesian filtering.
2. Doucet, A., and Johansen, A. M. A tutorial on particle filtering and smoothing: Fifteen years later. *Handbook of nonlinear filtering 12*, 656-704 (2009), 3.
3. Fan, S. The Light Curve Simulation and Its Inversion Problem for Human-Made Space Objects. Thesis.
4. Fan, S., and Frueh, C. A direct light curve inversion scheme in the presence of measurement noise. *The Journal of the Astronautical Sciences 67*, 2 (2020), 740–761.

5. FRIEDMAN, A., FAN, S., FRUEH, C., AND SCHILDKNECHT, T. Observability of light curve shape inversion based on optical data. In *First International Orbital Debris Conference* (2019).

6. GEWEKE, J. Bayesian inference in econometric models using monte carlo integration. *Econometrica: Journal of the Econometric Society* (1989), 1317–1339.

7. GOLDSTEIN, R., GOLDSTEIN, S., AND KESSLER, D. Radar observations of space debris. *Planetary and Space Science 46*, 8 (1998), 1007 – 1013.

8. HUDSON, R. S., AND OSTRO, S. J. Shape of asteroid 4769 castalia (1989 pb) from inversion of radar images. *Science 263*, 5149 (1994), 940–943.

9. KAASALAINEN, M. Asteroid models from photometry and complementary data sources. In *American Institute of Physics Conference Series* (May 2016), vol. 1732 of *American Institute of Physics Conference Series*, p. 020003.

10. KAASALAINEN, M., AND TORPPA, J. Optimization Methods for Asteroid Lightcurve Inversion. I. Shape Determination. *Icarus 153* (Sept. 2001), 24–36.

11. KAASALAINEN, M., TORPPA, J., AND MUINONEN, K. Optimization Methods for Asteroid Lightcurve Inversion. II. The Complete Inverse Problem. *Icarus 153* (Sept. 2001), 37–51.

12. KAASALAINEN, M., TORPPA, J., AND PIIRONEN, J. Models of Twenty Asteroids from Photometric Data. *Icarus 159* (Oct. 2002), 369–395.

13. KITAGAWA, G. Monte carlo filter and smoother for non-gaussian nonlinear state space models. *Journal of computational and graphical statistics 5*, 1 (1996), 1–25.

14. LIU, J. S., AND CHEN, R. Sequential monte carlo methods for dynamic systems. *Journal of the American statistical association 93*, 443 (1998), 1032–1044.

15. MORSELLI, A., DI LIZIA, P., BIANCHI, G., BORTOLOTTI, C., MONTEBUGNOLI, S., NALDI, G., PERINI, F., PUPILLO, G., ROMA, M., SCHIAFFINO, M., MATTANA, A., SALERNO, E., MAGRO, A., ADAMI, K. Z., ARMELLIN, R., SERGIUSTI, A. L., VILLADEI, W., DOLCE, F., REALI, M., AND PAOLI, J. A new high sensitivity radar sensor for space debris detection and accurate orbit determination. In *2015 IEEE Metrology for Aerospace (MetroAeroSpace)* (2015), pp. 562–567.

16. OLIKER, V., AND FRUEH, C. Stability of the Solution of the Minkowski Problem and its Application to Light Curve Inversion. in preparation.

17. SCHILDKNECHT, T., HUGENTOBLER, U., AND PLONER, M. Optical surveys of space debris in geo. *Advances in Space Research 23*, 1 (1999), 45 – 54.

18. SCHILDKNECHT, T., MUSCI, R., PLONER, M., BEUTLER, G., FLURY, W., KUUSELA, J., [DE LEON CRUZ], J., AND [DE FATIMA DOMINGUEZ PALMERO], L. Optical observations of space debris in geo and in highly-eccentric orbits. *Advances in Space Research 34*, 5 (2004), 901 – 911. Space Debris.

19. SILHA, J., SCHILDKNECHT, T., HINZE, A., FLOHRER, T., AND VANANTI, A. An optical survey for space debris on highly eccentric and inclined meo orbits. *Advances in space research 59*, 1 (2017), 181–192.

20. SMITH, A. *Sequential Monte Carlo methods in practice*. Springer Science & Business Media, 2013.